

## ATMOSPHERIC AIR AND NITROGEN DC GLOW DISCHARGES WITH THERMIONIC CATHODES AND SWIRL FLOW

Zdenko Machala<sup>\*</sup>, Christophe O. Laux<sup>†</sup>, and Charles H. Kruger<sup>‡</sup>

*Thermosciences Division, Mechanical Engineering Department, Stanford University, Stanford, CA 94305*

Graham V. Candler<sup>§</sup>

*Aerospace Engineering and Mechanics, University of Minnesota, Minneapolis, MN 55455*

### Abstract

Atmospheric air and nitrogen glow discharges have been studied in our laboratory over the past few years with an overall goal to produce nonequilibrium plasmas with high electron number densities (at least  $10^{12}$  cm<sup>-3</sup>) and relatively low gas temperatures (about 2000 K), as well as to meet the challenges of low power requirements and large plasma volumes. We now introduce a novel approach to produce highly ionized atmospheric pressure air and nitrogen plasmas in DC glow discharges. We employ thermionic cathodes (LaCrO<sub>3</sub>, LaB<sub>6</sub> and Mo) and place the discharges in tubes with swirl gas flow injection. As a result, an increase of the electron density by 1-2 orders of magnitude was achieved ( $10^{13}$ - $10^{14}$  cm<sup>-3</sup>), together with higher current densities and lower electric fields. The swirl flow confines the discharge, increasing its current and electron densities, enhancing its stability, and enabling it to extend to as long as 10 cm. A new falling region in the air discharge  $E$ - $j$  and  $E/N$ - $j$  characteristics was revealed. Computational analysis helps to understand the stabilizing effect of the swirl flow. DC discharges with thermionic cathodes combined with the swirl flow represent a promising way for producing scaled-up highly ionized atmospheric air or nitrogen plasmas.

### 1. Introduction

Large volume air and nitrogen plasmas at atmospheric pressure present considerable interest for a wide range of applications, such as electromagnetic wave shielding, air pollution control, biochemical decontamination, surface treatment, and plasma-assisted combustion. Generally speaking, desirable conditions are electron densities of at least in the order of  $10^{12}$  cm<sup>-3</sup> and gas temperatures below 2000 K. Our research focuses on air and nitrogen glow discharges at atmospheric pressure. These discharges have received renewed attention during the past few years.

Two main difficulties in the research on discharges at atmospheric pressure have been encountered, the power required to maintain such plasmas at atmospheric pressure, as well as their size. The power required to sustain the plasma with our previously studied direct-current (DC) discharges is relatively large ( $3$  kW/cm<sup>3</sup> for  $10^{12}$  electrons/cm<sup>3</sup>). The largest volumes obtained with our dual and multiple DC discharges were about  $1$  cm<sup>3</sup>.<sup>1</sup>

This paper focuses on DC discharges operating in air and nitrogen at atmospheric pressure with a novel approach of using thermionic cathode materials and swirl gas flows. It follows our previous AIAA paper<sup>1</sup> and other works<sup>2-6</sup> that progressively described experimental and theoretical investigations of DC and pulsed discharges in atmospheric pressure air and nitrogen.

In glow discharges with ordinary metal cathodes, the basic mechanisms of electron emission from the cathode are secondary processes such as positive ion impact. When a *thermionic cathode* is employed, its electron emission is enhanced by the thermionic effect induced by the elevated cathode temperature.

Section 2 describes our experimental facilities and techniques. Review of the previous experiments with atmospheric air and nitrogen discharges is given in Section 3. Section 4 describes our novel approach: discharges with thermionic cathodes and the swirl flow injection. Finally, Section 5 describes a computational analysis of the discharges in the swirl flow.

---

<sup>\*</sup> Postdoctoral Fellow, Member AIAA

<sup>†</sup> Professor, Ecole Centrale Paris, France, Associate Fellow AIAA

<sup>‡</sup> Professor, Member AIAA

<sup>§</sup> Professor, Associate Fellow AIAA

## **2. Experimental**

### **2.1. Discharge setup and cathodes**

Atmospheric glow DC discharges are obtained by applying a few hundred volts to a few kilovolts between ballasted electrodes. We employed a 15 kW DC power supply, Del High Voltage Model RHVS, delivering up to 10 kV and 1.5 A together with a ballast resistor of 3-50 k $\Omega$  in series with the discharge, as shown in Figure 1. The appropriate value of the ballast resistor was chosen according to the operating current in order to stabilize the discharge.

Two platinum pins parallel to the axis of the gas flow were previously used as electrodes. The pins were welded onto water-cooled stainless steel tubes. In experiments with thermionic cathodes, the cathode (typically the lower stainless steel tube with Pt pin) was replaced with a small piece of thermionic material. Lanthanum chromite (LaCrO<sub>3</sub>), lanthanum hexaboride (LaB<sub>6</sub>) and Molybdenum (Mo) were tested as thermionic materials. Mo is a hard metal, LaCrO<sub>3</sub> and LaB<sub>6</sub> are fragile, slightly conductive ceramics. All these materials are difficult to weld, especially the ceramics. In addition, we needed these special cathodes in the middle of the gas flow but allowing the gas to flow around them approximately uniformly.

The best technical solution for Mo cathode was to fix a 1-2 mm thin strip of Mo on top of the brass nozzle that provides the gas flow (nozzle exit diameter 1 cm). For ceramic cathodes, we used the copper or stainless steel mesh that covered the nozzle exit. A little, usually irregular, piece (~1-2 mm) of LaCrO<sub>3</sub> or LaB<sub>6</sub> was then fixed in the mesh in about the center of the gas flow, as shown in Figure 2. The thermionic cathodes were heated by the discharge itself.

Ceramic, glass and quartz tubes of various inner diameters (4.7; 8.38; 10.45; 15.5; 22.1 mm) and both swirl and axial gas injection into the discharge were examined to study their effects on the fluid dynamics of the plasma system. The swirling flow was established by tangential injection of the supply gas near the base of the microwave plasma torch in its off mode. In general, the tubes and the swirl flow help to stabilize the discharge spatially. Experiments in open air without the use of tubes were also conducted for comparison. Ceramic tubes can resist higher plasma temperatures but glass and especially quartz tubes enable valuable direct emission spectroscopy of the discharge inside the tube. We also performed experiments with ordinary metal cathodes and swirl flow in tubes in

order to elucidate separate roles of the thermionic and the swirl flow effects.

### **2.2. Optical diagnostics**

Temperature and electron number density measurements were made by means of spatially resolved optical emission spectroscopy. Spectra of the 2<sup>nd</sup> and 1<sup>st</sup> positive systems of N<sub>2</sub> (C<sup>3</sup> $\Pi_u$ -B<sup>3</sup> $\Pi_g$  and B<sup>3</sup> $\Pi_g$ -A<sup>3</sup> $\Sigma_u^+$ ), in some cases also NO  $\gamma$  (A<sup>2</sup> $\Sigma^+$ -X<sup>2</sup> $\Pi_r$ ) and N<sub>2</sub><sup>+</sup> 1<sup>st</sup> negative (B<sup>2</sup> $\Sigma_u^+$ -X<sup>2</sup> $\Sigma_g^+$ ) systems were used to determine the rotational and vibrational temperatures,  $T_r$  and  $T_v$ , respectively, using the SPECAIR radiation code<sup>7</sup>. In atmospheric pressure plasmas,  $T_r$  is close to the gas temperature owing to fast collisional relaxation. A schematic of the optical set-ups is shown in Figure 1. Two spectroscopic devices were used, each with appropriate optics.

The first system uses an Ocean Optics S2000 dual spectrometer, fitted with two grating/CCD combinations. The two 1200 and 600 grooves/mm gratings provide coverage of the two spectral ranges: 200-500 nm, and 400-1050 nm, with respective wavelength resolutions of 0.41 and 0.88 nm. We use two independent optical trains separated by a small angle and focused to the same point in the discharge, one for UV, and the other for VIS-NIR spectral region. In each train, light emitted from the discharge collected with two fused silica lenses is focused into a fiber optic connected to the respective spectrometer channel. The optical trains are mounted on a translation stage, which enables horizontal and vertical lateral scanning in both spectral regions simultaneously.

While the S2000 spectrometer described above provides quick but poorly resolved spectral scanning in the whole region between 200-1050 nm, we used an additional spectroscopic system providing better spectral resolution. It contains a 75-cm monochromator SPEX 750M (200-800 nm grating) fitted with a 2000x800 pixel CCD camera SPEX TE2000 (15x15  $\mu$ m pixel dimension). Both monochromator, and the CCD camera were controlled by a PC (National Instruments Labview programs). The light emitted from the discharge is collected with a spherical mirror, translated using the 4-mirror translational system, and then focused by another spherical mirror onto the entrance slit of the monochromator. The best wavelength resolution of this system is 0.04 nm; we typically use 0.12 nm resolution, which is satisfactory to resolve the rotational structure of molecular spectra. This system also provides 2-dimensional scanning capability. Furthermore, it allows taking wavelength-specific CCD camera images of the discharges that are useful for measuring the discharge diameter.

Absolute intensity calibrations for both spectroscopic systems were obtained by means of two radiance standards traceable to NIST calibrations. Both systems in their typical settings provide a spatial resolution

of 250  $\mu\text{m}$ . We also used a digital camera Nikon Coolpix 990 for documentation of discharges. The temperature of the thermionic cathodes was measured by the infrared pyrometer Minolta Land Cyclops 152.

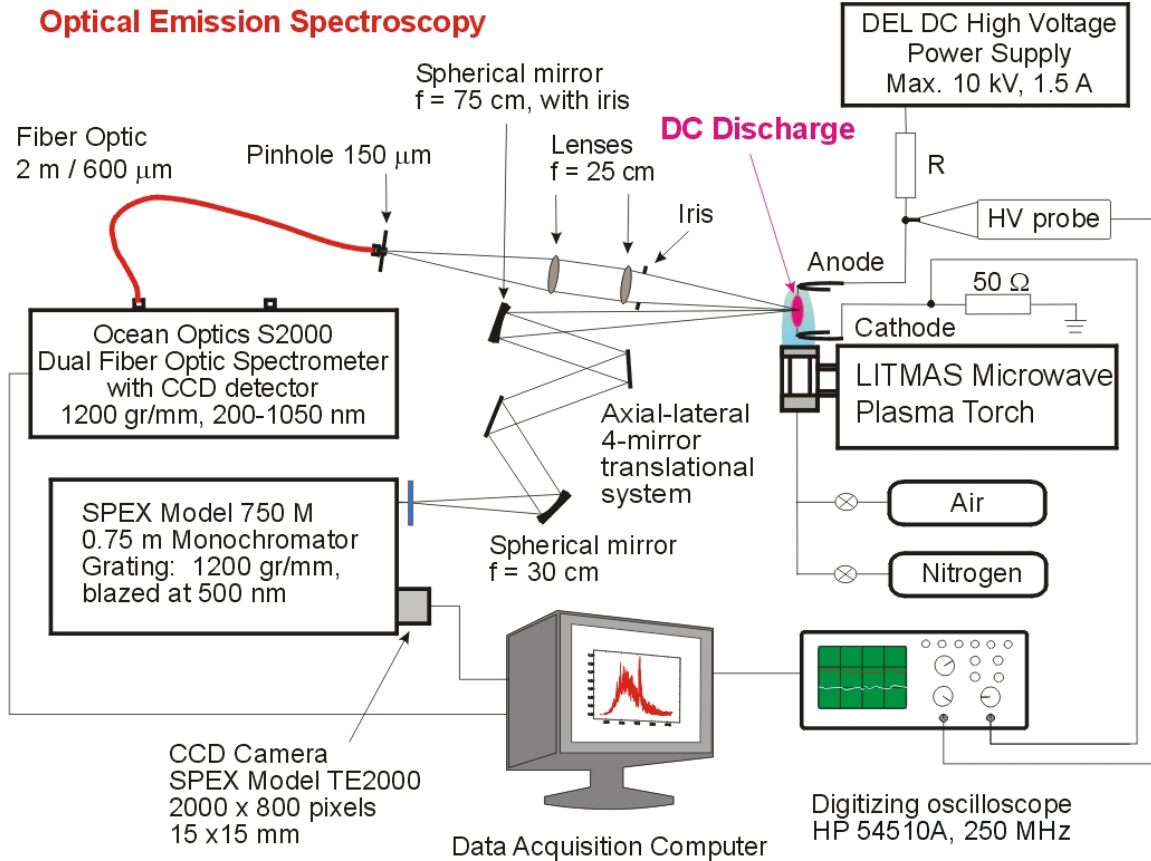


Figure 1. Overall view of the experimental setup for DC discharges and optical emission spectroscopy.

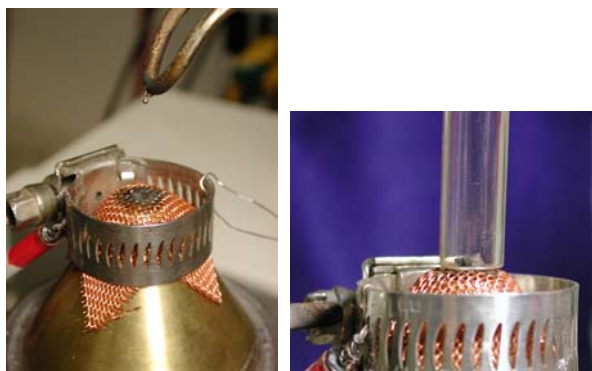


Figure 2. Setup for experiments with thermionic cathodes. A small piece of  $\text{LaCrO}_3$  or  $\text{LaB}_6$  ceramic is fixed on the copper mesh covering the top of the gas feeding nozzle. The same setup for glass/quartz tube experiments is on the right.

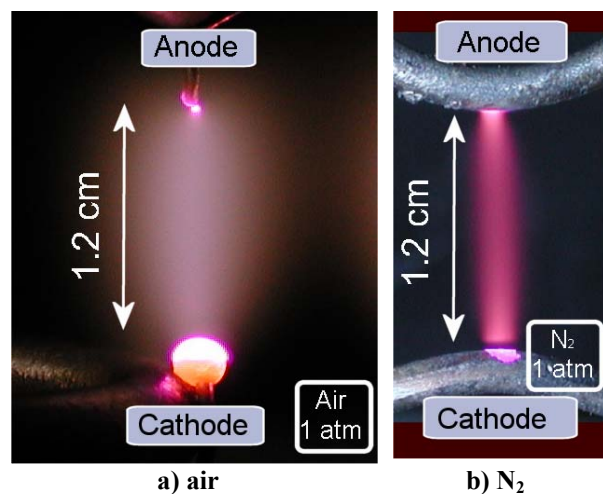


Figure 3. DC glow discharge in ambient atmospheric air and nitrogen ( $v = 0.5 \text{ m/s}$ ).  $I = 100 \text{ mA}$ ,  $U = 1.5 \text{ kV}$  in air,  $1.4 \text{ kV}$  in  $\text{N}_2$ .

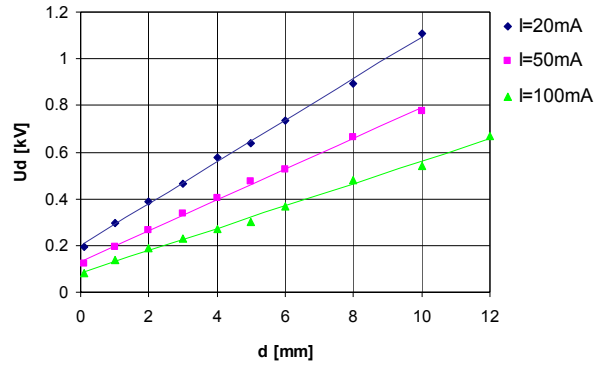


Figure 4. Discharge voltage as a function of interelectrode distance for various currents. The vertical offset on  $U_d$ -axis represents the cathode fall.

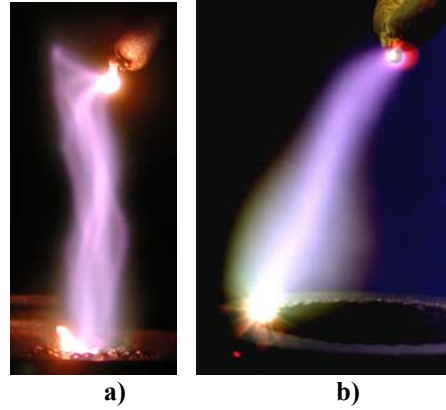


Figure 6. Discharge in open air with a)  $\text{LaCrO}_3$ , b)  $\text{LaB}_6$  cathode. Interelectrode distance 2 cm, air flow rate 63 slpm,  $I = 500$  mA, discharge diameter 3.1 mm.



Figure 5. Air discharges with  $\text{LaCrO}_3$  cathode in glass tubes and swirl flow,  $Q = 110$  slpm. a) tube diameter 8.38 mm,  $I = 500$  mA,  $d = 6.5$  cm,  $U = 1037$  V, discharge diameter  $D = 1.8$  mm. b) tube diameter 10.5 mm,  $I = 200$  mA,  $d = 1.8$  cm,  $U = 825$  V,  $D = 1.4$  mm.

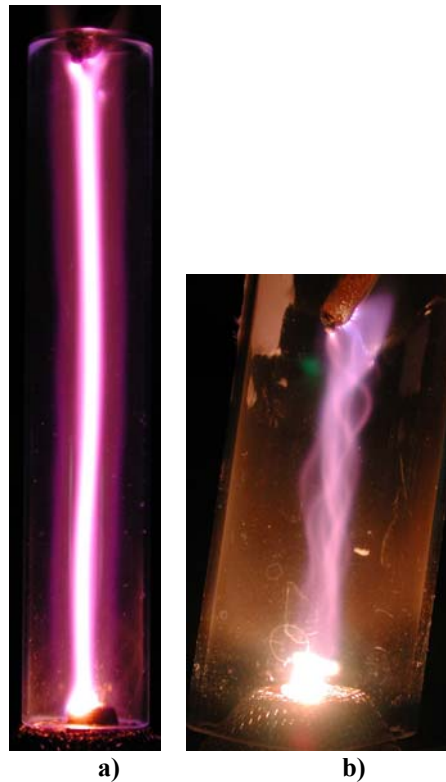


Figure 7. Nitrogen discharges with  $\text{LaCrO}_3$  cathode in glass tubes. a) Interelectrode distance  $d = 6$  cm, tube diameter 10.45 mm,  $Q = 110$  slpm,  $I = 200$  mA,  $U = 2144$  V, discharge diameter  $D = 1.6$  mm. b)  $d = 3.8$  cm, tube diameter 22.1 mm,  $Q = 110$  slpm,  $I = 500$  mA,  $U = 877$  V,  $D \approx 2.9$  mm.

### **3. Review of experiments with discharges in atmospheric air and nitrogen**

DC glow discharges in air and nitrogen at atmospheric pressure have been extensively studied at Stanford University over the past few years, both experimentally and theoretically.<sup>1-6</sup> The objective of these studies was to demonstrate the feasibility of stable atmospheric DC glow discharges without arcing that can generate relatively large volumes of nonequilibrium air (or nitrogen) plasmas, as well as to provide a clear understanding of the mechanisms of ionization and recombination in atmospheric pressure air plasmas.

#### **3.1. DC discharges in ambient air**

Figure 3a shows a photograph of a typical DC glow discharge in ambient air at atmospheric pressure with platinum electrodes. A DC glow discharge in nitrogen at the same conditions is shown for comparison (Figure 3b). The gas (air or nitrogen) is injected at about 0.5 m/s between two Pt electrodes separated by 1.2 cm. The air discharge voltage and current are 1.5 kV and 100 mA, respectively. The stratification into dark and bright layers typical of low pressure glow discharges is observed here at atmospheric pressure. Note for instance the darker region near the cathode (lower electrode) in the nitrogen discharge (Figure 3b) which can be assigned to Faraday dark space. Nevertheless, the cathode layers are concentrated in the immediate vicinity of the cathode, thus suggesting that the positive column occupies most of the interelectrode space. This observation was confirmed by electrical measurements. The electric field is found to be uniform in the interelectrode space, except within the close vicinity to the cathode. The voltage drop across the cathode region is about 280 V, a value typical of the cathode fall in air glow discharges with Pt electrodes.<sup>8</sup>

The diameter of the discharge in air measured by emission spectroscopy of the  $N_2$   $C^3\Pi_u-B^3\Pi_g$  (0,0) transition at 337 nm is approximately 1.7 mm for the current of 100 mA. The same discharge diameter was measured for the nitrogen discharge of the same conditions. Since the C state of  $N_2$  is produced by electron-impact excitation, this diameter is representative of the region with high electron number density. In Figure 3, the discharge in air appears to be wider than the discharge in nitrogen. This effect is due to the presence of a halo around the discharge produced by  $NO_2$  emission in the surrounding air environment heated by the discharge. The measured gas temperature in the discharge channel at these conditions is about 2500 K, and the estimated electron temperature is around 9500 K. This thermal nonequilibrium provides further indication that the discharge is a glow and not an arc.

The DC glow discharges in ambient air flows can be operated in the current range from 2 to several hundreds of mA. The corresponding gas temperatures, measured by optical emission spectroscopy at the centerline of the discharge column, are in the range 1500-4000 K, and depend strongly on the gas velocity. The current-voltage characteristic of the discharges in ambient air is descending. The gap length can be varied up to several cm, depending on the gas flow velocity and the discharge current.

The conductivity, hence the electron number density, can be obtained using Ohm's law and the measured electric field strength and current density (determined from the measured discharge current and discharge diameter).<sup>2-3</sup> We estimated the electron number density  $n_e$  to be in the order of  $10^{12}$   $cm^{-3}$ . In experiments with pure  $N_2$ , the value obtained by this method agrees well with the  $n_e$  measured by Cavity Ring-Down Spectroscopy of  $N_2^+$ , the dominant ion in nitrogen glow discharges.<sup>6</sup>

#### **3.2. DC Discharges in fast flow of preheated air**

DC discharge experiments were also conducted in a fast flowing air preheated at  $\sim 2000$  K. Microwave and RF plasma torches described in detail in Ref. <sup>1-4</sup> were used to preheat the gas. The main reason for going to fast gas flows (20-400 m/s) is that discharges in slow flows result in significant gas heating, especially at high currents where electron number densities of  $10^{12}$   $cm^{-3}$  or higher are achieved. The mechanism of gas heating can be explained as follows.

In the DC discharges, a large fraction of the electron energy is lost via excitation of the vibrational modes of air molecules, mainly  $N_2$ . These vibrational modes subsequently relax through collisions with the dominant species, i.e. O,  $N_2$ , and  $O_2$ . This collisional quenching transfers the energy from vibration into the translational modes of molecules, which results in Joule heating of the gas. This process is called vibrational-translational energy transfer (VT transfer). In slow air flows, the residence time of the gas in the discharge is long enough to enable the VT transfer. As a result, the gas is heated.

In fast air flows, on the other hand, the vibrational modes of  $N_2$  have a shorter time to relax, hence they cannot heat the gas as much over the short residence time between the two electrodes. Thus the temperature in the discharge approaches the temperature of the inlet gas. However, it is difficult to maintain stable DC discharges in fast flows of ambient air. This is because at ambient temperature, electron attachment is fast, whereas ionization is slow since the reduced field strength  $E/N$  (where  $E$  is the field strength and  $N$  is the

gas density) is lower due to the lower gas temperature, hence higher  $N$ .

For these reasons, we used a fast flow of pre-heated air at  $\sim 2000$  K. At this temperature, electron attachment does not play an important role. Moreover, the density is about seven times lower than at room temperature and the reduced field strength  $E/N$  is sufficient to maintain the discharge. When the residence time of the flow in the discharge column is shorter than the characteristic time for VT relaxation, the temperature remains close to 2000 K.

#### **4. Discharges with thermionic cathodes and swirl flow**

A *thermionic cathode* emits electrons by thermionic emission, i.e. electron emission induced by elevated temperature. In glow discharges with ordinary metal cathodes, the basic mechanisms of electron emission from the cathode are secondary processes such as positive ion impact. When a thermionic cathode is employed, electron emission from the cathode is enhanced by the thermionic emission, as a function of cathode temperature.

We tested lanthanum chromite ( $\text{LaCrO}_3$ ), lanthanum hexaboride ( $\text{LaB}_6$ ) and Molybdenum ( $\text{Mo}$ ) as thermionic cathode materials because their thermionic effect starts at relatively low temperature ( $\sim 1400$ - $2000$  K). Although thermionic electron emission is often used in arcs, we still operate glow discharges producing nonequilibrium plasmas where the electron temperature is larger than the gas temperature, the latter being in the range of 2500-3500 K.

##### **4.1. Cathode fall reduction**

Typically, glow discharges have their characteristic high-field cathode fall region where the voltage drops steeply by several hundreds of volts in a relatively short distance near the cathode. This region is only a few tens of  $\mu\text{m}$  thick at atmospheric pressure. The cathode fall in glow discharges is a function of the cathode material and the gas.<sup>8</sup>

When thermionic electron emission takes place, the cathode fall is reduced. With increasing temperature of the cathode, the thermionic emission starts to prevail over the secondary emission and there is no longer a need for the cathode fall. This is advantageous from the point of view of power budget since the overall discharge voltage is reduced.

We have measured the discharge voltage  $U$  as a function of the interelectrode distance  $d$  at various currents  $I$ , using  $\text{LaCrO}_3$  thermionic cathode in atmos-

pheric air discharges (Figure 4). For every specific current  $I$ ,  $U$  depends on  $d$  linearly. The line slope which gives the electric field strength  $E$ , decreases as the  $I$  increases. The value where the line crosses the  $U$ -axis corresponds to the cathode fall, since the size of the cathode fall region is negligible when compared with the size of the positive column. One can observe that with thermionic cathodes, the cathode fall value decreases with the rising  $I$ , unlike in regular glow discharges where it only depends on the cathode material and the gas. This is due to the thermionic cathode emission that amplifies with increasing cathode temperature depending on the current. We find that at currents over 200 mA, the  $\text{LaCrO}_3$  cathode temperature gets over  $\sim 1800$  K and the cathode fall is eliminated.

##### **4.2. Discharges with $\text{LaCrO}_3$ and $\text{LaB}_6$ cathodes in open air**

Figure 6 shows 2 cm long DC discharges with  $\text{LaCrO}_3$  and  $\text{LaB}_6$  cathodes in open ambient air (without any tube) with the flow rate  $Q = 63$  slpm (standard liters per minute). For both cases, the  $I = 500$  mA. The  $U = 447$  V or 420 V, resulting in a relatively low electric field strength  $E = 224$  V/cm or 210 V/cm, respectively for  $\text{LaCrO}_3$  and  $\text{LaB}_6$  cathodes (cathode fall is close to 0 in both cases). Cathode temperature measured by the infrared pyrometer is found to be about 2100 K for  $\text{LaCrO}_3$  and 1500 K for  $\text{LaB}_6$ , while anode temperature is about 1600 K in either case. The discharge diameter measured in the middle of the vertical axis and defined by the half width at half maximum of the emission intensity profiles of molecular bands of  $\text{N}_2$  (B-A) and atomic lines of Cr and O is found to be around 3 mm for both cases, for  $\text{LaB}_6$  also measured from the BO emission. By making a simplified calculation assuming a constant current density distribution across the whole discharge diameter, we get the current density  $j = 7$  A/cm<sup>2</sup> for both cases. The power density  $P = jE$  is relatively low (about 1.5 kW/cm<sup>3</sup>). The gas temperature in the middle of the discharge channel measured as rotational temperature of the molecular bands of  $\text{N}_2$  (B-A) system is  $T_g \approx 3000$  K. The estimated electron number density  $n_e$  in both discharges is high, approximately  $3 \times 10^{13}$  cm<sup>-3</sup>, and is one order of magnitude higher than a typical value obtained in DC discharges with Pt cathodes.

The discharge diameter is slightly increased when the current  $I$  is increased, though not enough to keep  $j$  constant, so  $j$  increases with the increasing  $I$ . On the other hand, the electric field  $E$  decreases with increasing  $I$  in such a manner that the resulting power density  $P = jE$  does not increase. This seems to be a reason why discharges with thermionic cathodes often have lower power requirements (per number of elec-

trons created) than those with regular metal cathodes: a lower  $E$  is needed to sustain the discharge.

#### **4.3. Effect of tubes and swirl gas flow**

Discharges in open air tend not to be spatially and temporally uniform (Figure 6a). This makes their spectroscopic diagnostics, as well as measuring their precise diameter and consequently current density, difficult. In order to stabilize them we put them in the tubes. Tubes with various inner diameters have been tested ( $\Phi = 4.7; 8.38; 10; 10.45; 15.5; 22.1$  mm). They were placed directly on top of the gas supplying nozzle with 1 cm diameter exit, as shown in Figure 2b.

Tubes with a large diameter ( $\Phi = 22.1$  mm) do not seem to have much effect on the discharge stability and straightness. On the contrary, tubes with medium and small diameters ( $\Phi = 15.5; 10.45; 10; 8.38$  mm) affect the discharge considerably. The spatial and temporal uniformity of the discharge is improved. In addition, the discharge can undergo higher gas flow rates of ambient air or nitrogen without extinguishing. Furthermore, the discharge is more confined in the middle of the tube, its diameter  $D$  is reduced when compared with open air cases. Because of the reduced  $D$ ,  $j$  is increased, and consequently,  $n_e$  and  $P$  are increased as well.

Figure 5 shows the 6.5 and 1.8 cm long discharges in ambient air swirl flow with the flow rate  $Q = 110$  slpm and tubes of 8.38 and 10.5 mm inner diameter. Their parameters are, respectively:  $I = 500$  and 200 mA,  $E = 160$  and 458 V/cm,  $D = 1.8$  and 1.4 mm,  $j = 20$  and 13 A/cm<sup>2</sup>,  $n_e \approx 10^{14}$  and  $3 \times 10^{13}$  cm<sup>-3</sup>. Both discharges have  $T_g \approx 3000$  K.

The smallest diameter tubes ( $\Phi = 4.7$  mm), in which the gas flow velocity is the highest, confine the discharge to the greatest extent. However, their use is technically limited because the hot discharge easily touches the glass/quartz tube wall and melts it.

We also studied the effect of the tube diameter on the discharge properties in nitrogen swirl flow. The same behavior was observed, namely the tubes improve the discharge stability, enable them to operate at higher flow rates, and cause confinement of the discharge channel resulting in increased  $j$ ,  $P$ , and  $n_e$ . The smaller the tube diameter and the higher the gas flow rate, the smaller discharge diameter is measured. Figure 7 shows the discharges in ambient swirl nitrogen flow in glass tubes with following characteristics, respectively:  $d = 6$  and 3.8 cm;  $I = 200$  and 500 mA;  $\Phi = 10.45$  and 22.1 mm;  $Q = 110$  and 94 slpm;  $E = 365$  and 231 V/cm. The discharge in the glass tube with small diameter (Figure 7a) is straighter, narrower and more stable, al-

lowing to reliably measure its diameter and other parameters:  $D = 1.6$  mm;  $j = 10$  A/cm<sup>2</sup>;  $n_e \approx 3 \times 10^{13}$  cm<sup>-3</sup>;  $P = 3.6$  kW/cm<sup>3</sup>. On the other hand, the discharge in the large diameter tube (Figure 7b) is broader and less uniform, with filaments; we were thus not able to measure its diameter reliably.

We have also explored the effect of the swirl gas injection in comparison with axial gas injection. Discharges with axial gas injection are much more sensitive to the gas flow rate. They are stable only at low gas flow rates (max.  $Q = 21$  slpm for  $I = 200$  mA). They also have larger column diameters than their counterparts in the swirl flow because they are not confined. The discharge diameter in axial flow does not depend on the tube diameter; the tubes have no effect here.

These observations indicate that the swirl gas flow, especially in narrow tubes at high gas flow rates, is responsible for unique fluid dynamic properties in the tube. We assume that the swirling gas flows at the fastest speed close to the tube walls, whereas the flow is slower in the middle of the tube. Such flow properties stabilize the discharge in the middle of the tube because it can more easily heat the gas by the VT transfer mechanism described in Section 3.2. In addition, pressure is probably slightly reduced in the core of the tube. Consequently, the reduced field  $E/N$  in the core of the tube must be higher, thus stabilizing the discharge in this central zone. Further computational analysis of this problem is presented in Section 5.

Note that the gaps of 6.5 cm in Figure 5 or 6 cm in Figure 7 are very long. We have easily operated 10 cm discharges in tubes with the swirl gas flow. Such long discharges were not possible to obtain without using the stabilizing effect of the swirl flow and the tube. Operating in this configuration is therefore interesting from the point of view of plasma volume scaling.

#### **4.4. Discharges with Mo cathode in swirl flow**

Discharges with a Mo thermionic cathode are similar to those with LaCrO<sub>3</sub> or LaB<sub>6</sub> cathodes. According to Raizer and Dobretsov<sup>8-9</sup>, Mo is a less satisfactory thermionic material than La-based compounds, because the thermionic emission starts at higher cathode temperature. However, we have achieved thermionic emission from Mo cathode in air DC discharges. An example of such a discharge is shown in Figure 8. A 3.1 cm long discharge of  $I = 500$  mA and  $U = 781$  V is operated in the glass tube with 10.45 mm inner diameter. The ambient air is swirl-injected at  $Q = 110$  slpm. Measured discharge diameter in the mid-distance between the electrodes is only  $D = 1.3$  mm which results in the very high  $j = 38$  A/cm<sup>2</sup>

and  $n_e \sim 10^{14} \text{ cm}^{-3}$ . The electric field is low,  $E = 207 \pm 45 \text{ V/cm}$ , and the gas temperature measured spectroscopically was found to be  $2750 \pm 250 \text{ K}$ .

One can observe from Figure 8 that the discharge originates at the side of the Mo cathode strip, close to the glass tube wall. Then it slides almost horizontally along the surface of the Mo cathode and finally gets its vertical direction toward the anode. It is also obvious that the discharge is not uniformly thick; the  $D$  and  $j$  values provided in the above paragraph correspond to the middle of vertical axis where the discharge is the thinnest.

#### **4.5. Discharges with stainless steel cathodes in swirl flow**

After obtaining interesting results of experiments with thermionic cathodes combined with the swirl flow injection, the question arose: Are improved discharge properties mostly due the effect of the thermionic cathode or rather due to the effect of the swirl flow in tubes? In order to separate the two effects we performed some experiments with the discharges with ordinary metal cathodes (stainless steel) but using the swirl flow and the tubes.

Interestingly, we have found that stable long discharges could be obtained in swirl flow in tubes even with non-thermionic cathodes. These discharges have similar properties to those with thermionic cathodes and swirl flow, achieving high  $j$  and  $n_e$ , but typically operate at slightly higher  $E$ . The gas temperature measured in these cases is high:  $\sim 3500 \text{ K}$ . These discharges are very stable, even though their length can exceed 10 cm.

#### **4.6. Spectra of discharges with thermionic cathodes**

Open air discharges with Pt, stainless steel or Cu cathodes typically used to exhibit  $\text{N}_2$  2<sup>nd</sup> (C-B) and 1<sup>st</sup> (B-A) positive systems, NO  $\gamma$  system and OH A-X bands, their relative intensities depended on the discharge parameters. The 2<sup>nd</sup> positive system of  $\text{N}_2$  is the most convenient for determination of rotational and vibrational temperatures, as well as for measurements of the discharge diameter from the emission intensity profiles. Unfortunately, this system was found to be very weak or absent in most of the air discharges with thermionic cathodes, as well as in the discharge with stainless steel cathode with the swirl flow. This is probably due to the low electric field that is not high enough for electron-impact excitation of the  $\text{N}_2$   $\text{C}^3\Pi_u$  state (11 eV). The absolute value of the emission intensity of  $\text{N}_2$  2<sup>nd</sup> positive system normalized to the discharge diameter as a function of the  $E/N$  is shown in

Figure 9. The emission intensity increases approximately exponentially with the  $E/N$ .

The  $\text{N}_2$  1<sup>st</sup> positive system typically appears in the VIS-NIR spectrum from thermionic cathode discharges. The electric field is probably still sufficient to excite the  $\text{N}_2$   $\text{B}^3\Pi_g$  state by the electron impact (7.4 eV). An example of a UV spectrum of a 500 mA discharge with  $\text{LaCrO}_3$  cathode compared with a 5 mA discharge with Cu cathode is shown in Figure 10.

In our first set of experiments with thermionic cathodes and glass tubes with swirl flow, we developed a novel technique using the  $\text{N}_2$  1<sup>st</sup> positive system for temperature measurement since this was often the only distinguished molecular system. Yet, this system is very complex, especially in nonequilibrium plasmas where nonequilibrium vibrational distributions change relative intensities of their particular bands. It is not generally used for temperature measurements. Furthermore, the high wavelength tail of VIS-NIR spectra was raised by the wall reflections of a very intense continuum radiation from the thermionic cathode. The complexity of the spectrum of an air discharge with  $\text{LaCrO}_3$  cathode is illustrated on the sample VIS-NIR spectrum in Figure 11.

We have chosen a part of the 1<sup>st</sup> positive  $\text{N}_2$  system spectrum between 875-884 nm which corresponds to transitions between vibrational levels close to each other and still has a reasonable intensity to be distinguished from the cathode continuum radiation. We have assumed that these transitions are not too affected by vibrational nonequilibrium and that the slope can be used for determination of rotational temperature after careful zero adjustments and normalization. The reliability of this technique was verified on various non-thermionic cathode experiments with distinct  $\text{N}_2$  2<sup>nd</sup> positive spectra. The best obtained accuracy of this technique applied to thermionic cathode discharges was  $\pm 250 \text{ K}$ . In many cases where the signal-to-noise ratio was low, we were only able to measure by this way with an accuracy of  $\pm 500 \text{ K}$ , or unable to measure at all.

Later we upgraded glass tubes with quartz tubes, enabling us to detect UV molecular systems such as NO  $\gamma$  and OH A-X that could be used for temperature measurements. These spectra also provided further verification of the  $T_g$  measurement technique based on  $\text{N}_2$  1<sup>st</sup> positive system.

Strong atomic Cr or Mo lines appear in the spectra of the discharges with  $\text{LaCrO}_3$  and Mo cathodes, Fe and Cr lines in the spectra of discharges with stainless steel cathode, and O lines in all cases. In the discharges with  $\text{LaB}_6$  cathodes, we detected a new molecular system in VIS region that we assigned to BO

(boron monoxide), Figure 12. In general, the lack of  $N_2$  2<sup>nd</sup> positive system and perturbing atomic or molecular lines make the spectroscopic diagnostics of these discharges difficult.



Figure 8. Air discharge with Mo cathode in 10.45 mm thick glass tube, interelectrode distance 3.1 cm,  $Q = 110$  slpm,  $I = 500$  mA,  $U = 781$  V, discharge diameter 1.3 mm.

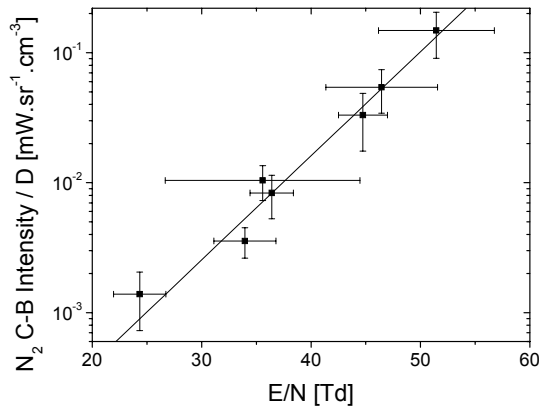


Figure 9. Absolute emission intensity of  $N_2$  (C-B) normalized to the discharge diameter  $D$  as a function of  $E/N$ .

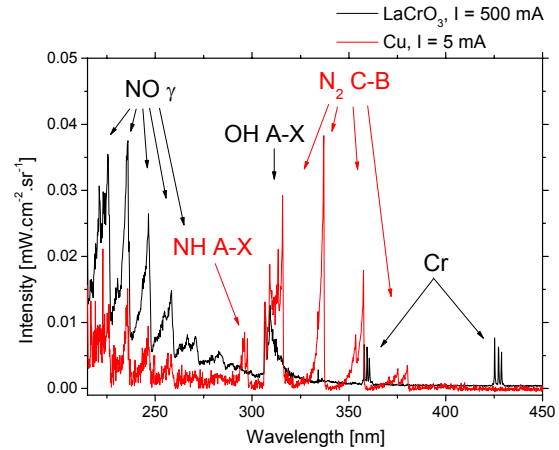


Figure 10. UV emission spectrum of air discharge with  $LaCrO_3$  cathode at  $I = 500$  mA compared with air discharge with Cu cathode at  $I = 5$  mA.  $LaCrO_3$  discharge properties are the same as in Figure 5a.

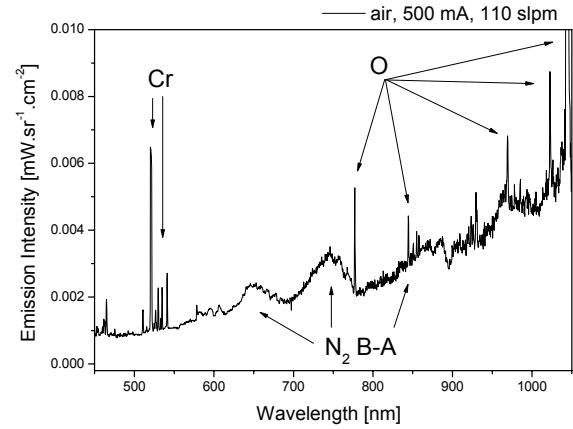


Figure 11. VIS-NIR emission spectrum of air discharge with  $LaCrO_3$  cathode. Discharge properties are the same as in Figure 5a.

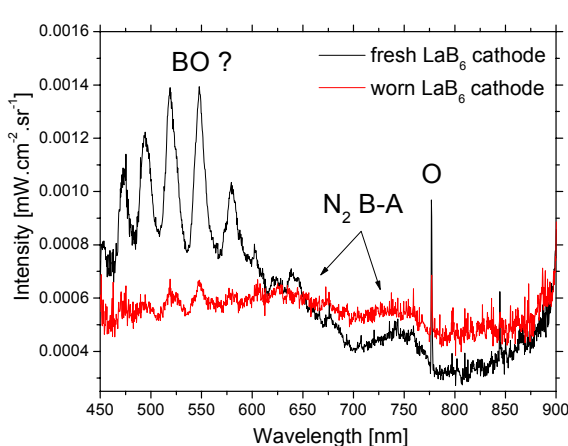


Figure 12 VIS-NIR emission spectrum of air discharge with  $\text{LaB}_6$  cathode, fresh vs. worn cathode.  $I = 100$  mA.

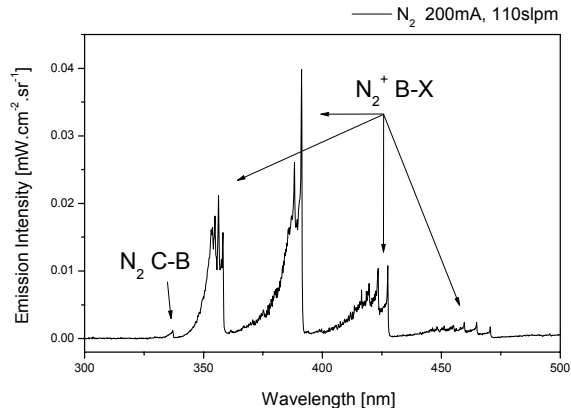


Figure 13. UV-VIS emission spectrum of  $\text{N}_2$  discharge with  $\text{LaCrO}_3$  cathode. Discharge properties are the same as in Figure 7a.

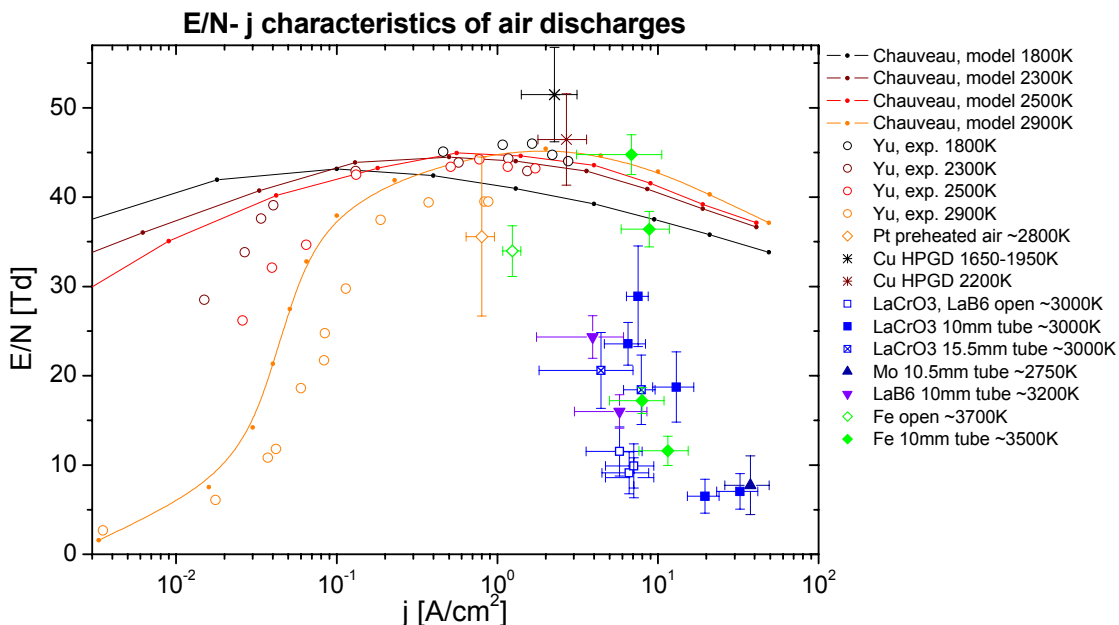


Figure 14.  $E/N$ - $j$  characteristics of air discharges. Solid lines: collisional-radiative modeling by Chauveau<sup>10</sup>; experimental data designated Yu: discharges in preheated air with Pt cathodes<sup>2</sup>. Open symbols: experiments in open ambient air; full symbols: experiments in tubes with vortex flow of ambient air.

On the other hand, perturbing atomic Cr, Mo, Fe and O lines provide a useful tool for discharge diameter measurements. The presence of Cr, Mo and Fe lines in the air spectra with  $\text{LaCrO}_3$ , Mo and steel cathodes, as well as the presence of BO with  $\text{LaB}_6$  cathode, indicate the degradation of the cathode. This effect was confirmed by two other observations: deposits on the

tube walls and reduction of the cathode material size up to its complete disappearance after a certain time of operation. The surface structure of the cathode material apparently changes during the operation, especially with Mo cathodes that become covered by the white-yellowish layer of Mo oxide (most likely  $\text{MoO}_3$ ).  $\text{LaB}_6$  cathodes, although generally considered one of the best thermionic materials, do not seem to be very conven-

ient for our strongly oxidizing hot air conditions. They only operate for few minutes and quickly degrade, releasing BO and leaving white amorphous-like deposit on the cathode. Figure 12 also shows different magnitudes of the BO emission intensity when the cathode is fresh and when it has already been used for few minutes. Out of the materials we tested,  $\text{LaCrO}_3$  seems to be the most convenient thermionic material for atmospheric air discharges, capable of functioning for several hours without substantial degradation.

The nitrogen discharges with  $\text{LaCrO}_3$  cathode provide completely different spectra. First, there are no atomic Cr or O lines present. Apparently, chromium is neither sputtered nor evaporated like in the air discharges. This is probably due to chemically inert  $\text{N}_2$  gas, whereas oxidation of  $\text{LaCrO}_3$ , as well as  $\text{LaB}_6$  and Mo occurs in air. Second,  $\text{N}_2$  1<sup>st</sup> positive system is much more intense than in air discharges. It is thus easier to use it for diagnostic purposes. Third, a strong  $\text{N}_2^+$  1<sup>st</sup> negative system appears in the UV spectra. Its emission indicates a high degree of ionization, hence high  $n_e$ . An example of such a spectrum in the UV is shown in Figure 13.

#### **4.7. General $E$ - $j$ characteristics of air discharges**

General voltage-current characteristics of DC atmospheric air discharges represented in terms of electric field – current density ( $E$ - $j$ ) have been reported previously.<sup>2-4</sup> Experimental points on an  $E$ - $j$  graph were shown together with numerical predictions of collisional-radiative model of nonequilibrium air plasmas, also developed in our research group.<sup>10-11</sup> Now we put our new experimental data together with all previous data on these characteristics. The reduced field – current density ( $E/N$ - $j$ ) representation is more appropriate because it accounts for the temperature variations in various experiments. The gas temperature in most of the experiments with the swirl flow was around 3000 K.

The new experimental data referring to discharges with thermionic cathodes and swirl flow fall in the lower right portion of the  $E/N$ - $j$  graph in Figure 14. These discharges operate at lower  $E/N$  and higher  $j$  than the previously explored discharges with Pt or Cu cathodes. The new data reveal a falling trend of the tail of  $E/N$ - $j$  curves; the same applies for the  $E$ - $j$  characteristic. Decreasing  $E/N$  is associated with decreasing emission intensity of the  $\text{N}_2$  (C-B) system, as shown in Figure 9. If we assume that the  $\text{N}_2$  C state is mainly populated by direct electron impact, i.e. its population is proportional to  $T_e$ , and depopulated by radiation to the  $\text{N}_2$  B state, this result may then indicate decreasing  $T_e$  with increasing  $n_e$ . It would be consistent with our previously re-

ported S-shaped behavior of the  $T_e$ - $n_e$  curve.<sup>2-4</sup> However, other depopulation mechanisms of  $\text{N}_2$  C may take place and possibly overwhelm the  $\text{N}_2$  C-B radiation. Quenching by O atoms may be such a mechanism since the concentration of O atoms is likely to be considerably high at high  $n_e$ . A detailed analysis of all possibly involved elementary processes should be considered in our present collisional-radiative model in order to associate the falling trend of  $E/N$ - $j$  curve with the  $T_e$ - $n_e$  curve and draw reliable conclusions.

In discharges with thermionic cathodes and swirl flow, we observe a significant enhancement of the electron density, the estimated  $n_e$  of these discharges is  $\sim 10^{13}$ - $10^{14}$   $\text{cm}^{-3}$ , i.e. 1-2 orders of magnitude higher than the previously obtained  $n_e$  in the discharges with metal cathodes in open air. At the same time, the power requirements per electron created are lower.

Variation of experimental conditions (with or without tubes, various tube diameters, swirl vs. axial flow, cathode materials, etc.) causes a relatively large scatter of these data, especially in terms of  $j$ . However, some common features can be found:

- For a fixed  $E$  and  $E/N$ ,  $j$  is greater in the experiments with tubes and the swirl flow (full points in Figure 14) than in open air experiments, regardless to the cathode material. This is caused by the previously discussed discharge confinement due to the swirl flow.
- For a given  $j$ ,  $E$  and  $E/N$  are lower in the experiments with thermionic cathodes (blue and violet points in Figure 14) than in the experiments with metal cathodes, regardless to the flow conditions. We find here low  $E$  and  $E/N$  even when the cathode fall was subtracted when we calculated the  $E$  and  $E/N$  in experiments with metal cathodes (cathode fall is reduced with thermionic cathodes, as discussed in section 4.1).

At present, we do not fully understand the separate roles of the thermionic effect and the swirl flow. It seems that the swirl flow effect is more important from the viewpoint of high  $n_e$  (due to the discharge confinement) and of the discharge stability, hence volume scaling.

### **5. Computational analysis of discharges in swirl flow**

The swirl-stabilized discharge was modeled using a computational fluid dynamics method that simulates the key physical processes occurring in the flow. The method solves the Navier-Stokes equations augmented to include finite-rate reactions and internal

energy relaxation, as well as energy addition due to the electric field. We use an 11-species (N<sub>2</sub>, O<sub>2</sub>, NO, O, N, O<sub>2</sub><sup>+</sup>, N<sub>2</sub><sup>+</sup>, NO<sup>+</sup>, N<sup>+</sup>, O<sup>+</sup>, e) finite-rate air chemistry model, including a two-temperature ( $T$ ,  $T_e$ ) representation of the ionization reactions.<sup>4</sup> The governing equations and numerical method are discussed, and the computed results are then presented.

The solution of the full set of conservation equations (including mass conservation for each of the eleven species present, momentum equations in the axial, radial, and swirl directions, and internal energy equations for vibrational energy, electron translational energy, and total energy) is very challenging at the high electron temperature and atmospheric pressure conditions considered here. For an explicit calculation, the stable time step is dictated by the rate of ionization, Joule heating, and energy exchange. From experience, the stable time step is typically 0.1 ns, while the characteristic flow time is of the order of 200 μs; thus steady-state solutions require a huge number of time steps. Attempts to derive implicit formulations have been partially successful, resulting in time step increases of the order of 50 over explicit methods. However, the effect of using an implicit method on the time-accuracy of these flows is unknown, and therefore only an explicit time-integration method was used here.

To date, the full discharge code is only partially successful at predicting the state of the discharge. However, complete solutions of the swirling flow have been obtained to give estimates of  $E/N$  in the discharge region.

### 5.1. Governing equations

The electron conservation equation is given by:

$$\frac{\partial n_e}{\partial t} + \nabla \cdot \vec{j}_e = \omega_e$$

where  $\omega_e$  is the rate of formation of electrons by reactions. The electron number flux,  $\vec{j}_e$ , is obtained from the electron momentum equation by neglecting inertia. This gives:

$$n_e \vec{v}_e = \vec{j}_e = -n_e \mu_e \vec{E} - \frac{D_e}{T_e} \nabla (n_e T_e)$$

where  $D_e$  is the electron diffusion coefficient and  $\mu_e$  is the electron mobility. Now, for numerical reasons,<sup>12</sup> it is more convenient to write the electron velocity in terms of the logarithmic derivative of the electron number density:

$$\vec{v}_e = -\mu_e \vec{E} - \frac{D_e}{T_e} \nabla T_e - D_e \nabla (\ln n_e)$$

This form results in significantly less numerical error in regions where the electron number density is changing rapidly. In one dimension, the numerical representation of the electron conservation equation becomes:

$$n_{e,i}^{n+1} = n_{e,i}^n - \frac{\Delta t}{\Delta x} (n_{e,i+1/2}^n v_{e,i+1/2}^n - n_{e,i-1/2}^n v_{e,i-1/2}^n) + \Delta t \omega_{e,i}^n$$

where  $n_{e,i+1/2}$  is the cell-face average electron number density, and  $v_{e,i+1/2}$  is computed using the electron temperature and number density at grid points  $i$  and  $i+1$ . This approach is easily extended to multiple dimensions.

The electron energy equation is given by:

$$\begin{aligned} \frac{\partial}{\partial t} \left( \frac{3}{2} n_e k T_e \right) + \nabla \cdot \left( \frac{5}{2} n_e k T_e \vec{v}_e \right) = & -n_e e \vec{E} \cdot \vec{v}_e \\ - n_e \sum_h 3k [(T_e - T) + (T_e - T_v) \delta_{eh}] \frac{m_e}{m_h} v_{eh} - & \omega_e I + \nabla \cdot (\lambda_e \nabla T_e) \end{aligned}$$

where  $I$  is the average energy supplied by the electrons to the ionization reactions, and  $\lambda_e$  is the electron thermal conductivity. The energy exchange term represents the rate of energy loss from the electrons to the heavy particles through elastic collisions and through inelastic interactions primarily with the nitrogen vibrational modes. We account for the inelastic energy loss through the inelastic loss factor,  $\delta_{eh}$ , which is from Ref.4. A similar numerical method is used for this equation, with the electron velocity evaluated using the logarithmic derivative.

It should be noted that in the direction perpendicular to the electric field, the electrons and ions diffuse as pairs. Thus, the electron diffusion coefficient in the field-normal direction is given by the ion diffusion coefficient. However, the electron thermal diffusivity is not changed by this ambipolar diffusion approximation.

The electric field can be computed from the Poisson equation for the electric potential. However, we choose to take advantage of the experimental geometry, and assume that the field only varies in the direction along the axis of the glass tube. In this case, there is no forced diffusion in the radial direction, which simplifies the implementation of the numerical method outlined above. In addition, we can determine the local electric field from the known total current of the discharge. Fundamentally, we know

$$I = - \int_A e n_e v_e dA = \int_A e n_e \left( \mu_e E_x + \frac{D_e}{T_e} \frac{\partial T_e}{\partial x} + D_e \frac{\partial \ln n_e}{\partial x} \right) dA$$

where  $A$  is the cross-sectional area of the discharge and

$v_e$  is the axial electron velocity. Now, since the total current is a parameter set by the experimental conditions, we can compute the electric field at each axial location from the above equation. This ensures that the discharge carries the correct current at every location. This concept is supported by previous work cited in Raizer.<sup>8</sup>

The above equations are coupled to the heavy particle mass conservation equations, the vibrational energy conservation equation, and the total energy conservation equation, and are solved using a finite-volume method. Because the flow field has a significant component of swirl, we solve a swirl momentum equation under the assumption that the flow is axisymmetric. We use an 11-species finite-rate air chemistry model, including a two-temperature ( $T$ ,  $T_e$ ) representation of the ionization reactions.<sup>4</sup> The coupling between the electrons and the heavy particle flow takes place primarily through the energy exchange terms.

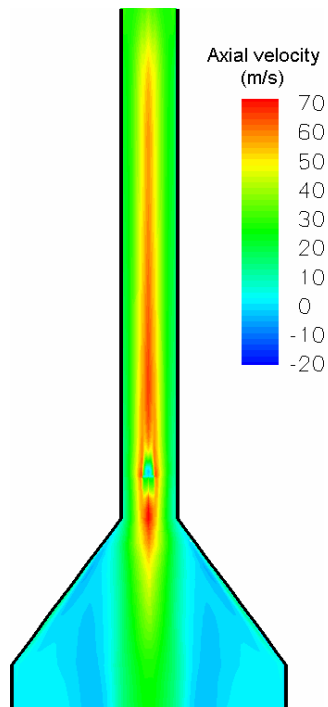


**Figure 15. Contour of the axial velocity in the 10 mm thick tube with a DC discharge ( $I = 500$  mA).**

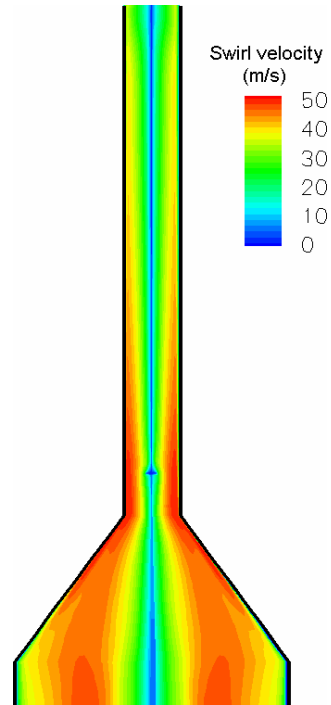


**Figure 16. Contour of the swirl velocity in the 10 mm thick tube with a DC discharge ( $I = 500$  mA).**

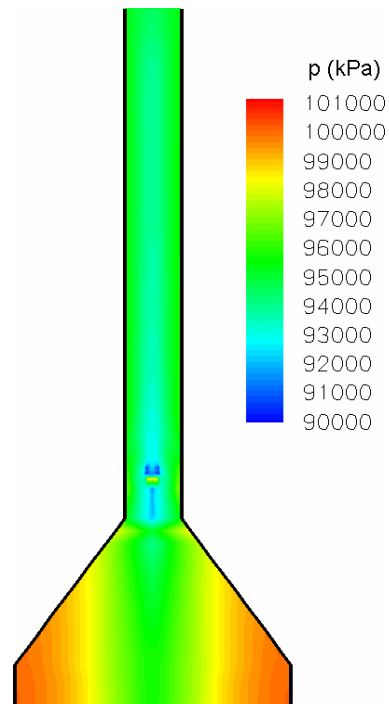


**Figure 17. Contour of the pressure in the 10 mm thick tube with a DC discharge ( $I = 500$  mA).**

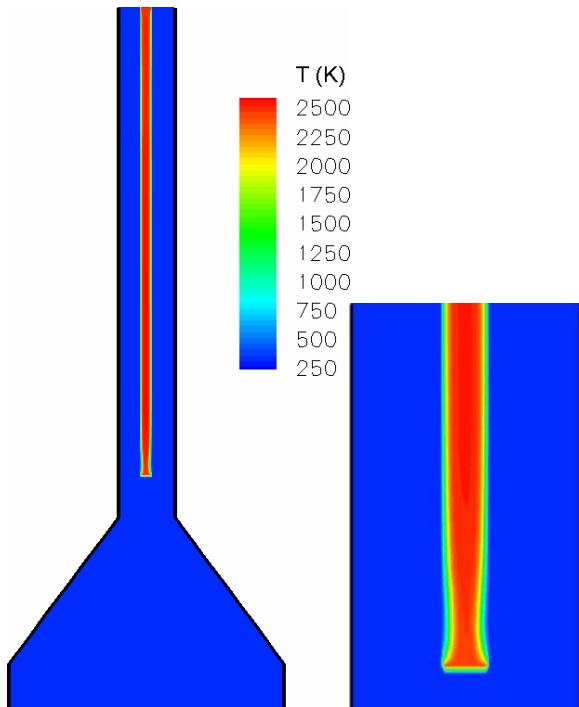


Figure 18. Contour of the gas temperature in the 10 mm thick tube with a DC discharge ( $I = 500$  mA), zoomed section at right.

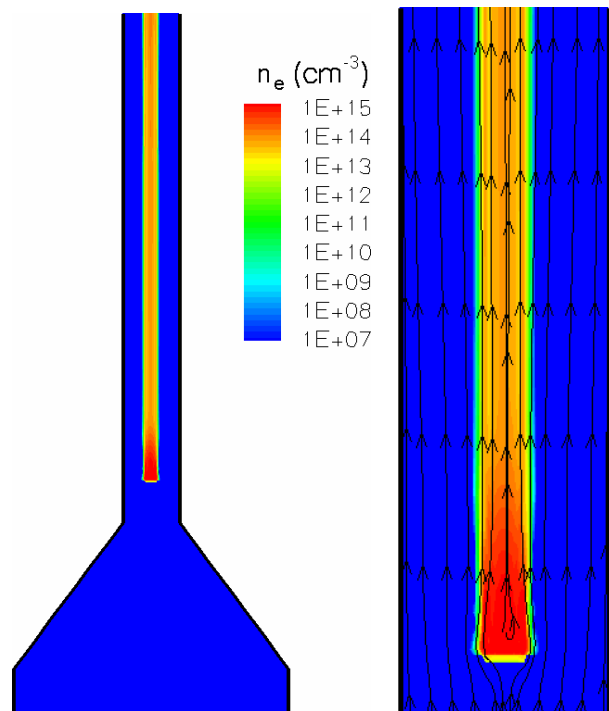


Figure 20. Contour of the electron density in the 10 mm thick tube with a DC discharge ( $I = 500$  mA), zoomed section at right.

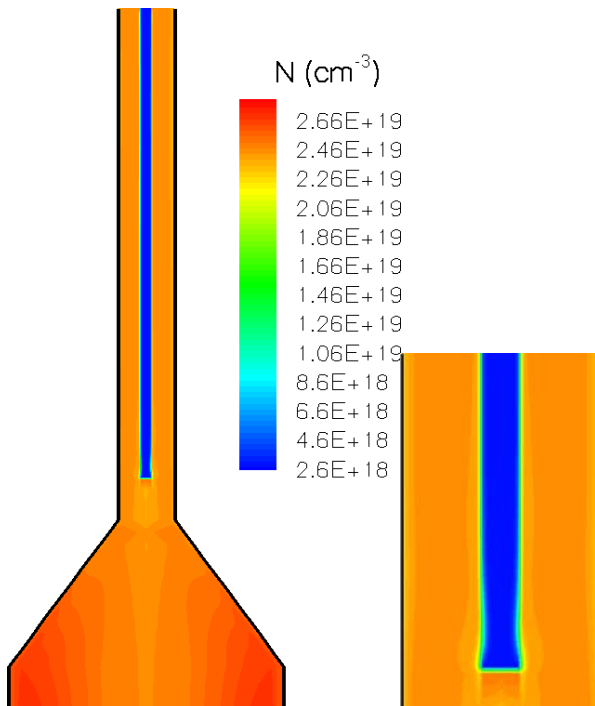


Figure 19. Contour of the gas density in the 10 mm thick tube with a DC discharge ( $I = 500$  mA), zoomed section at right.

## 5.2. Discharge conditions

In the computational analysis, we considered a representative DC discharge with  $I = 500$  mA, operated in a 10 mm diameter tube with tangential injection of ambient air at  $Q = 110$  slpm. The interelectrode distance was set to 6 cm.

The experimental configuration introduces the supply air by radial injection near the base of the cylindrical test section that is ended on top with the nozzle supplying the gas into the discharge tube. We simulate this injection through the use of mass, swirl momentum and energy source terms at the injection locations. The outflow pressure at the exit of the glass test tube is specified, and the flow field is then allowed to evolve until a steady-state flow is established. We then numerically ignite the discharge by providing a region of elevated temperature and electron concentration between the electrodes. The governing equations are then integrated in time until a steady discharge is established.

The cathode was represented in the middle of the discharge tube, 1 cm above the nozzle exit. The model does not account for the cathode material. The thermionic effect is thus not considered, but no cathode

fall was implemented that is typical for the thermionic cathodes in our conditions, as discussed in section 4.1.

The cathode boundary conditions are critical to establishing the discharge. The cathode provides a flux of electrons corresponding to the known current. Therefore, for a given cathode dimension, the electron number or mass flux is known, and can be imposed at the grid points that represent the cathode. Within the finite volume cells that represent the cathode, we can compute the electron number density from the equation given above. Finally, we must assume an electron temperature within these cells; we take this value to be 2500 K. However, this assumption is not critical because the electron temperature increases rapidly due to Joule heating.

### **5.3. Computational results and discussion**

Results of the computational analysis are represented in Figure 15-Figure 20 as color contours of relevant parameters. We show the converging nozzle and the 10 mm diameter discharge tube on its top, some figures also show a zoomed section of the discharge close to the cathode.

Figure 15 and Figure 16 show the contours of the axial and swirl flow velocity. While the axial velocity is the highest in the discharge zone due to elevated temperature, the swirl velocity is the lowest there. The strongest swirl is found close to the tube walls, especially in the low part of the discharge zone.

Figure 17 and Figure 18 show the contours of the pressure and the gas temperature. We observe a slight (max. 10 %) pressure drop in the discharge zone. The gas temperature is increased up to  $\sim 2500$  K in the discharge zone. This is in a fairly good agreement with the measured gas temperatures that were typically about 3000 K. The region of the high temperature is relatively uniform, as can be seen from the zoomed section in Figure 18, and confined in the middle of the tube.

Figure 19 represents the gas density contours. Because of slightly reduced pressure and strongly elevated temperature, the  $N$  drops 10 times in the discharge zone, compared to normal conditions. The region of the low  $N$  is fairly uniform and confined in the middle of the tube. The lowered  $N$  causes a large enhancement of the reduced field  $E/N$  in the discharge zone. We assume that this is the key phenomenon that keeps the discharge confined in the middle of the tube and makes it very stable, even at large gap distances.

In Figure 20, we show the contour of the electron density. The  $n_e \sim 10^{14} \text{ cm}^{-3}$  is achieved in the discharge zone, which agrees well with the measured values for a 500 mA air discharge at these flow conditions.

Even higher  $n_e \sim 10^{15} \text{ cm}^{-3}$  is found close to the cathode. Although we did not measure the  $n_e$  in this region, such a result is physically possible, because many electrons are emitted from the cathode (especially thermionic one), and the equilibrium between their generation and losses may have not yet been reached in this region. The computational results for the electron temperature are unfortunately not reliable at the present.

## **6. Conclusions**

In the first part of the paper we provided a review of the experiments with DC discharges in ambient and preheated air and nitrogen. These discharges are able to produce nonequilibrium air and nitrogen atmospheric pressure plasmas with electron densities of the order of  $10^{12} \text{ cm}^{-3}$  and gas temperatures about 2000 K. We emphasized the mechanism of gas heating via vibrational-translational (V-T) energy transfer because it is found to significantly influence the discharge properties.

In the following part, we introduced a novel approach to produce highly ionized atmospheric pressure air and nitrogen plasmas by DC glow discharges. In this approach, we used thermionic cathodes and the swirl gas flow injection. We investigated various thermionic cathodes materials ( $\text{LaCrO}_3$ ,  $\text{LaB}_6$  and Mo). We also tested the effects of the swirl flow in the discharges placed in tubes, compared with the axial flow, and the tube diameter effects. As a result of both thermionic emission and swirl flow effects, an increase of the electron density by 1-2 orders of magnitude was achieved (up to  $10^{13}$ - $10^{14} \text{ cm}^{-3}$ ), together with the high current densities  $j$  and the low electric fields  $E$  and reduced fields  $E/N$ , when compared to previously investigated discharges in open air/nitrogen and metal cathodes. Use of small diameter tubes with the swirl flow results in the discharge confinement, and consequently an electron density increase, regardless to the cathode material. At these conditions, the discharges are very stable even at high flow rates of ambient air or nitrogen. They can be extended between the electrodes to as long as 10 cm, which is interesting from the point of view of plasma volume scaling.

In addition, use of the thermionic cathodes results in the lower  $E$  and  $E/N$  for a given  $j$ . Consequently, the power budget of these highly ionized plasmas, related to the electron density, is lower than in their previously investigated counterparts with ordinary cathodes. New experimental data are in the falling region of our previously reported air discharge  $E$ - $j$  and  $E/N$ - $j$  characteristics.

Emission spectroscopy diagnostics of air discharges with thermionic cathodes is challenging because the  $N_2$  (C-B) molecular system and other systems convenient for temperature measurements are weak or absent. In addition, atomic Cr, Mo and Fe lines, or molecular BO system, appearing due to sputtering/evaporation of the cathode material, perturb the spectra. We have developed a novel technique for rotational temperature measurement based on the  $N_2$  1<sup>st</sup> positive system (B-A).

In the last part of the paper, we present a computational analysis of DC discharges in a tube with the swirl flow. Computational fluid dynamics method including finite-rate reactions and internal energy relaxation, as well as energy addition due to the electric field was employed. The computational results are in a good agreement with the experiments. The gas density spatial distribution related to the  $E/N$  distribution helps to understand the discharge confinement and its stability in the tube with swirling gas. Numerically predicted high values of the  $n_e$  also agree well with experimental estimates.

The new experiments and computations indicate that use of thermionic cathodes combined with the swirl flow stabilization represent a promising way for producing nonequilibrium superionized plasmas in air or nitrogen at atmospheric pressure, as well as for scaling up the plasma volumes.

### **Acknowledgements**

This work was funded by the Director of Defense Research & Engineering (DDR&E) and by the Air Force Office of Scientific Research under the cognizance of Dr. Robert J. Barker. We gratefully acknowledge LITMAS, Inc. for loaning us the Litmas Red microwave torch.

### **References**

- [1] Z. Machala, C.O. Laux, X. Duten, D.M. Packan, L. Yu, C.H. Kruger: "Scaled-up Nonequilibrium Air Plasmas," 41<sup>st</sup> Aerospace Sciences Meeting and Exhibit, January 2003, Reno, NV, AIAA paper 2003-874
- [2] L. Yu, C. O. Laux, D. M. Packan, and C. H. Kruger, "Direct-Current Glow Discharges in Atmospheric Pressure Air Plasmas," J. Appl. Phys. **91**, 2678, 2002
- [3] C. H. Kruger, C. O. Laux, L. Yu, D. M. Packan, and L. Pierrot, "Nonequilibrium Discharges in Air and Nitrogen Plasmas at Atmospheric Pressure," Pure and Applied Chemistry **74**, 337, 2002
- [4] C. O. Laux, L. Yu, D. M. Packan, R. J. Gessman, L. Pierrot, and C. H. Kruger, "Ionization Mechanisms in Two-Temperature Air Plasmas," AIAA Paper 99-3476, June 1999
- [5] X. Duten, D. M. Packan, L. Yu, C. O. Laux, and C. H. Kruger, "DC and Pulsed Glow Discharges in Atmospheric Pressure Air and Nitrogen," IEEE Trans. Plasma Sci. Special Issue on "Images in Plasma Science" **30**, 178, 2002
- [6] A. P. Yalin, C. O. Laux, C. H. Kruger, and R. N. Zare, "Spatial Profiles of  $N_2^+$  Concentration in an Atmospheric Pressure Nitrogen Glow Discharge," Plasma Sources Sci. Technol. **11**, 248, 2002
- [7] C. O. Laux, "Optical Diagnostics and Radiative Emission of Air Plasmas," Ph.D. Thesis, Mechanical Engineering, Stanford, CA: Stanford University, 1993
- [8] Y. P. Raizer, "Gas Discharge Physics," New York: Springer, 1991
- [9] L. N. Dobretsov, M. V. Gomoiunova "Emission Electronics," Jerusalem, Israel program for scientific translations, 1971
- [10] S. M. Chauveau, C. O. Laux, J. D. Kelley, and C. H. Kruger, "Vibrationally Specific Collisional-Radiative Model for Nonequilibrium Air Plasmas", 33<sup>rd</sup> AIAA Plasmadynamics and Lasers Conference, Maui, HI, May 2002, AIAA paper 2002-2229
- [11] S. M. Chauveau, J. D. Kelley, C. O. Laux, and C. H. Kruger, "Vibrationally Specific Modeling of Nonequilibrium Effects in air Plasmas", 41<sup>st</sup> Aerospace Sciences Meeting and Exhibit, January 2003, Reno, NV, paper AIAA 2003-137
- [12] E.P. Hammond, K. Mahesh, and P. Moin, "A Numerical Method to Simulate Radio-Frequency Plasma Discharges," J. Computational Physics **176**, 402, 2002